Applied Catalysis B: Environmental 138–139 (2013) 304–310

Contents lists available at SciVerse ScienceDirect

Applied Catalysis B: Environmental

journal homepage: www.elsevier.com/locate/apcatb

Controllable synthesis of double layered tubular CdSe/ZnO arrays and their photoelectrochemical performance for hydrogen production

Meng Wang, Jiangang Jiang, Guanjie Liu, Jinwen Shi, Liejin Guo*

International Research Centre for Renewable Energy & State Key Laboratory of Multiphase Flow in Power Engineering, Xi'an Jiaotong University, Shaanxi 710049, China

ARTICLE INFO

Article history:
Received 6 November 2012
Received in revised form 26 January 2013
Accepted 3 February 2013
Available online 27 February 2013

Keywords:
CdSe/ZnO
Double layered structure
Photoelectrochemical
Hydrogen production

ABSTRACT

CdSe sensitized ZnO nanostructure arrays with double layered tubular structure were first synthesized by chemical bath deposition and chemical etch process with hydrothermal-synthesized ZnO nanorods as the template. CdSe/ZnO arrays with different micro-nanostructures like nanocable or double layered nanotube were obtained by changing chemical bath deposition conditions. Physicochemical and electrical properties of this novel material were investigated to describe its photoelectrochemical performance in an electrode cell. Under the irradiation of 100 mW/cm^2, CdSe/ZnO with double layered tubular structure gave maximum photocurrent of 2.55 mA/cm^2, which is over 12 times larger than that of bare ZnO. The high performance of this material was believed structure dependent. The structure effect and growth mechanism of the double layered nanostructure arrays were also discussed in this paper.

1. Introduction

Most conventional energy sources are getting exhausted because of the growing needs from the developing human society. Therefore searching for novel renewable and abundant energy sources is in crucial necessary. Among those potential sources that have been investigated, hydrogen has attracted much attention for its specific properties such as high thermal value, storability and environmental-friendliness. Efficient hydrogen production from water using photocatalysts has become one of the most attractive ways, since hydrogen and oxygen production from TiO_2 film was reported in 1972 [1]. Hereafter, numerous materials have been investigated such as metal oxides [2–8,42], metal sulphide [9–13], and metal nitride [14–16], and so on. In addition, metal oxides were extensively studied for its excellent properties such as low-toxicity, stability and facility. But stable metal oxides photocatalysts (such as TiO_2 and ZnO) usually have a wider band gap more than 3.0 eV. Therefore, they can only utilize ultraviolet light which accounts for only 4% of the solar spectrum. Important attempts have been concentrated on utilizing the visible part of the solar spectrum. For example: (1) metal ions and non metal ions have been doped to reduce the band gap energy of metal oxide semiconductors or to improve their electronic properties [17–19], (2) sensitizing metal oxide semiconductors with organic dyes is also an efficient way to expand their absorption edges [20,21], (3) narrow band gap semiconductor quantum dots like CdS, CdSe and CdTe have been used to form heterojunction with broad band gap metal oxides to utilize visible light and to improve separation efficiency of photo-generated charges [22–25]. The third way was widely developed over the past two decades. Olivia prepared CdS and CdSe sensitized mesoporous-TiO_2 films obtained by applying commercially P25 TiO_2 powder paste onto a FTO (fluorine-doped-tin oxide) glass, with common NH_3 bath and chemical bath deposition (CBD) method respectively. Both of the sensitized films exhibited markedly improved photoelectrochemical performance [26].

Semiconductors with 1D nanostructure like nanowire, nanorod or nanotube have excellent photoelectrochemical performance due to their high specific surface area and structure dependent properties [27]. Sensitizing 1D broad-band gap nanostructure arrays with narrow-band gap quantum dots have been proved to be one of the most valuable ways to achieve high-efficiency hydrogen production and pollution degradation. 1D ZnO nanorods with a band gap of 3.37 eV and a large excitation binding energy are promising photocatalytic materials, and are widely used in the sensitized solar cells [28]. Wang and co-workers prepared ZnO/CdTe core shell nanocable arrays on indium tin oxide (ITO glass) and the photocatalytic activity was investigated at the same time [29].

It is widely recognized that 1D nano-tubular nanostructure of ZnO exhibits higher porosity, larger surface area and excellent electron transport properties than bulk materials [30]. However, few reports focused on sensitizing ZnO nanotube with narrow band-gap quantum dots. In this study, a facile and controllable method was adopted to synthesize a double layered tubular structure composite with single crystal ZnO as the lining layer and

* Corresponding author. Tel.: +86 29 8266 3895.
E-mail address: lj-guo@mail.xjtu.edu.cn (L. Guo).

0926-3373/$ – see front matter © 2013 Elsevier B.V. All rights reserved.
http://dx.doi.org/10.1016/j.apcatb.2013.02.027

accumulated CdSe dots as the outer layer. To the best of our knowledge, this novel structure material was prepared for the first time. The physicochemical properties and photoelectrochemical performance of this material were both investigated. Moreover a possible growth mechanism was also prospected in this article.

2. Experimental

2.1. Synthesis procedure

(1) ZnO nanorod arrays were synthesized via a hydrothermal method similar to that described by Greene et al. [31] but with minor modification. The film was grown on fluorine-doped thin oxide (FTO) substrate. FTO coated glasses (TEC-15 15 Ω/sp) were cleaned by ultrasonic cleaning in acetone, de-ionized water and ethanol, and then dried under a stream of nitrogen. A solution of zinc acetate in methanol (0.1 mol/l) was spin-coated on FTO substrate at 2000 rpm for 25 s. Then the substrate was annealed in air at 350 °C for 30 min. The thus-obtained FTO glass with ZnO seeds was put into a mixed aqueous solution of zinc nitrate and hexamethylenetetramine (0.05 mol/l). Finally the solution was maintained at 90 °C for 20 h followed by calcination at 450 °C for 30 min.

(2) The depositing of CdSe quantum dots and the formation of double layered nanotube arrays were achieved by chemical bath deposition and chemical etch process. The Se source was from Na_2SeSO_3 which was prepared by dissolving 0.02 mol of selenium powder into aqueous solution (100 ml) of Na_2SO_3 (0.5 mol/l). Then the solution was maintained at 70 °C and refluxed for 5 h with a flow of nitrogen as the protection atmosphere. The thus-obtained Na_2SeSO_3 aqueous solution was stored at 60 °C in a conical beaker for further utilization. 0.505 g of KOH was added into 100 ml of de-ionized water with magnetic stirring. Then nitrilotriacetic acid (0.57 g) was added into the solution until KOH was dissolved completely, followed 30 min of stirring. Then 0.617 g of $Cd(NO_3)_2{\cdot}4H_2O$ was added into the solution with magnetic stirring for 5 min. The resulting transparent solution was maintained at reaction temperature for 30 min, before ZnO nanorod arrays was placed into the solution at a certain angle, 10 ml of Na_2SeSO_3 solution was added into the solution which was maintained for different time. The samples were described as CdSe/ZnO-*A*-*B*, *A* and *B* present temperature and time respectively.

2.2. Characterization

X-ray diffraction (XRD) patterns were obtained on a PANalytical X'pert MPD Pro X-ray diffractometer using Ni-filtered Cu Kα irradiation (Wavelength 1.5406 Å). The transmission spectra of the samples were determined with a Hitachi U-4100 UV-vis-near-IR spectrophotometer. The sample morphology was observed by a JEOL JSM-6700FE scanning electron microscope and a JEOL JEM 2100 transmission electron microscope. Elemental analysis for various samples was conducted by the OXFORD INCA energy-dispersive X-ray detector (EDX), which was mounted in a JEOL JSM-6700FE scanning electron microscope.

2.3. Photoelectrochemical measurement

Electrochemical and photoelectrochemical measurements were carried out in a convenient three electrodes cell. Work electrodes were made of the CdSe/ZnO arrays, and mounted onto a special designed electrode holder. The surface areas exposed to electrolyte were fixed at 0.785 cm^2. A silver chloride electrode was used as a reference electrode and a large area platinum plate was used as a counter electrode. Aqueous solution of Na_2S (0.1 M) was prepared as the electrolyte. A potentiostat 273A from Princeton Applied Research Company (PARC) and a 500 W Xe lamp (100 mW/cm^2) were used for photocurrent measurement and incident photon to current conversion efficiency (IPCE). The spectrogram of the Xe lamp was shown in Fig. S5. Photocurrent action spectra were recorded, and the absolute intensity of the incident light was recorded with an avaspec-2048 fiber optic spectrometer from Avnantes. The IPCE is calculated according to the formula in Ref. [41] as follows:

$$IPCE = \frac{hc}{e}\frac{I_{ph,\lambda}}{P_\lambda \lambda} \quad (1)$$

where $I_{ph,\lambda}$ is the photocurrent density, P_λ is the power intensity of the light, and h, c, and e have their usual meanings of Planck's constant, speed of light in vacuum, and elementary charge, respectively.

3. Results and discussion

3.1. Structure and morphology

Fig. 1 and Fig. S1 display the FESEM images of hydrothermally synthesized ZnO and CdSe/ZnO nanostructure arrays. The ZnO nanorods with the crystal structure of wurtzite were vertically grown on the FTO substrate. Diameter of the nanorods was about 100 nm as can be seen from Fig. S1a. ZnO nanorods were grown with smooth top surface ({0 0 0 2} planes) and side surface ({1 0 1 0} planes) [31]. After treatment with chemical bath deposition, different nanostructures, such as nanorod, nanocable, nanotube were formed which (Fig. 1a–d). When the reaction temperature and time were 30 °C and 60 min respectively, the several CdSe dots were deposited on the ZnO nanorods (inset, Fig. 1a). Fig. 1b shows the SEM image of CdSe/ZnO when reaction temperature reached to 40 °C. The amount of CdSe deposited on ZnO increased and the central part of ZnO began to dissolve into the reaction solution. When the reaction temperature increased to 60 °C, the central part of ZnO dissolved more severely to form a tubular structure. Therefore, the double layered nanostructure arrays were obtained with ZnO single crystal nanotube as the lining layer and accumulated CdSe quantum dots as the outer layer. Fig. 1d shows the image of CdSe/ZnO nanostructure arrays prepared at 60 °C for 100 min. Long reaction time lead to more remarkable dissolving of ZnO resulting in a more obvious tubular morphology.

Fig. 2 and Fig. S2 present the TEM and HRTEM (high resolution electron microscope) images of CdSe sensitized ZnO nanostructure arrays. The CdSe quantum dots were deposited on ZnO nanorods in the process of chemical bath deposition. The surface of ZnO became rough as the reaction temperature and reaction time increased. At 30 °C, little amount of CdSe quantum dots adhered to the ZnO nanorods, and the ZnO had not been etched in such reaction condition (inset, Fig. 2a). The HRTEM image of CdSe/ZnO-30-60 was presented in Fig. 2a. The diameters of CdSe quantum dots were found to be about 7.0 nm (the red circles in Fig. 2a). D-spacing of the lattice fringes of the dots deposited on nanorod was 0.37 nm, matching the {1 0 1 0} planes of hexagonal CdSe [32]. The lattice fringes D-spacing of the rod was 0.26 nm, matching well with the {0 0 0 2} planes of hexagonal ZnO (PDF card: 01-089-0510). As the reaction temperature and time increased to 60 °C and 100 min respectively, more CdSe quantum dots were deposited on the outer layer of ZnO to form a tubular structure (Fig. S2), and etching effect was more severe. Fig. 2b presents the HRTEM image of CdSe/ZnO-60-100. The D-spacing of 0.37 nm for CdSe ({1 0 1 0} planes of hexagonal CdSe) and 0.26 nm for ZnO ({0 0 0 2} planes of hexagonal ZnO (PDF card: 01-089-0510)) could also be found in the image. From the high resolution transmission electron microscope images,

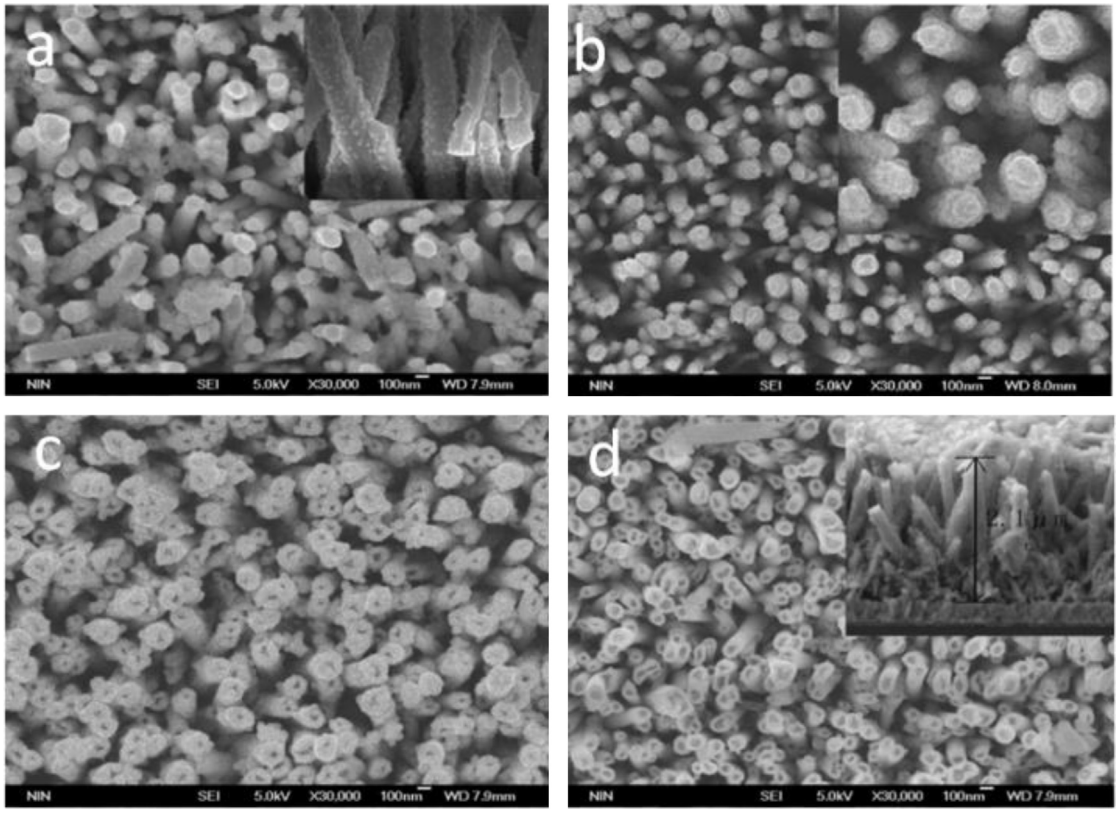

Fig. 1. High-powered SEM images of CdSe/ZnO double layered nanostructure arrays. (a) CdSe/ZnO-30-60, (b) CdSe/ZnO-40-60, (c) CdSe/ZnO-60-60 and (d) CdSe/ZnO-60-100.

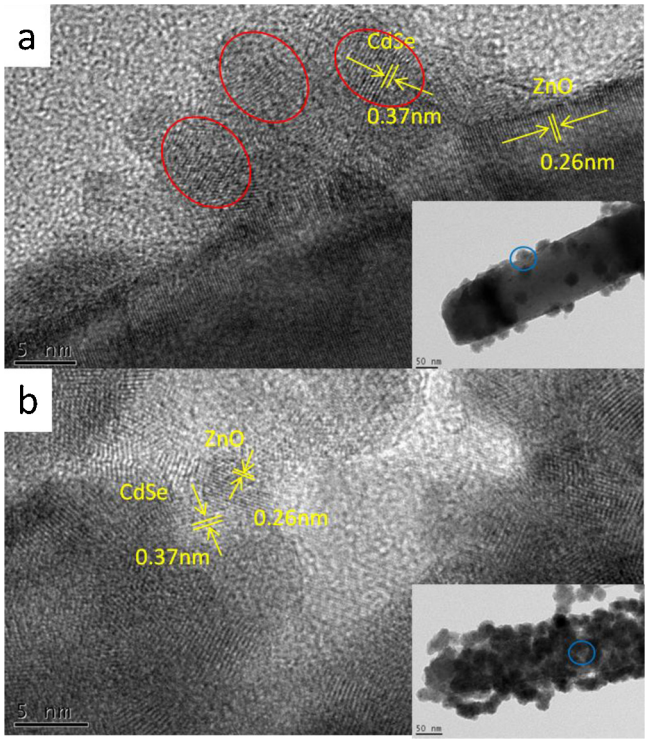

Fig. 2. TEM and HRTEM image of as-prepared CdSe/ZnO nanostructure arrays. (a) CdSe/ZnO-30-60 and (b) CdSe/ZnO-60-100. (For interpretation of the references to color in the text, the reader is referred to the web version of the article.)

distinct lattice fringes of CdSe and ZnO were observed. It shows that CdSe sensitized ZnO nanotube arrays prepared here were well crystallized in nature, which is necessary for high photocatalytic activity.

XRD patterns for CdSe/ZnO are presented in Fig. 3. Majority diffraction peaks were attributed to the hexagonal phase of ZnO. The most intensive diffraction peak was at 34.43° corresponding to the diffraction of (0 0 0 2) plane (PDF 01-089-0510), indicating that ZnO nanorods grew along the (0 0 0 1) direction which has already been proved by the SEM image (Fig. S1) and TEM image (inset, Fig. 2a). Diffraction peaks for CdSe which was illustrated in Fig. 3b were also found. Compared to CdSe/ZnO-30-60, the ZnO diffraction intensity of CdSe/ZnO-60-100 declined markedly (Fig. S3). The reason is that longer reaction time and higher reaction temperature aggravated the etching of ZnO rods. The growth mechanism of CdSe/ZnO films will be discussed subsequently.

3.2. Growth mechanism

Fig. 4 displays the growth mechanism of CdSe/ZnO nanostructure arrays. The reason for the double layered nanostructure formation is the synchronous process of CdSe depositing on the surface of ZnO and the etching of central part of ZnO rods. Schema 1 shows the depositing process when reaction temperature was low (for example 30 °C). CdSe dots started to be deposited on the ZnO surface, and the center of ZnO rods did not dissolve in the chemical bath solution, which can be seen in Fig. 2a. When reaction temperature and reaction time increased, more CdSe were deposited onto the ZnO surface, and a tubular structure was formed by the stacking of CdSe quantum dots around ZnO rods, which is illustrated in schema 2 (Fig. 4). Hexagonal ZnO is composed by O^{2-} and Zn^{2+} ions stacking alternatively along the *c*-axis, which presents a top surface of (0 0 0 1)-O and a bottom surface of (0 0 0 1)-Zn [33]. So the top surface and bottom surface of ZnO have higher surface

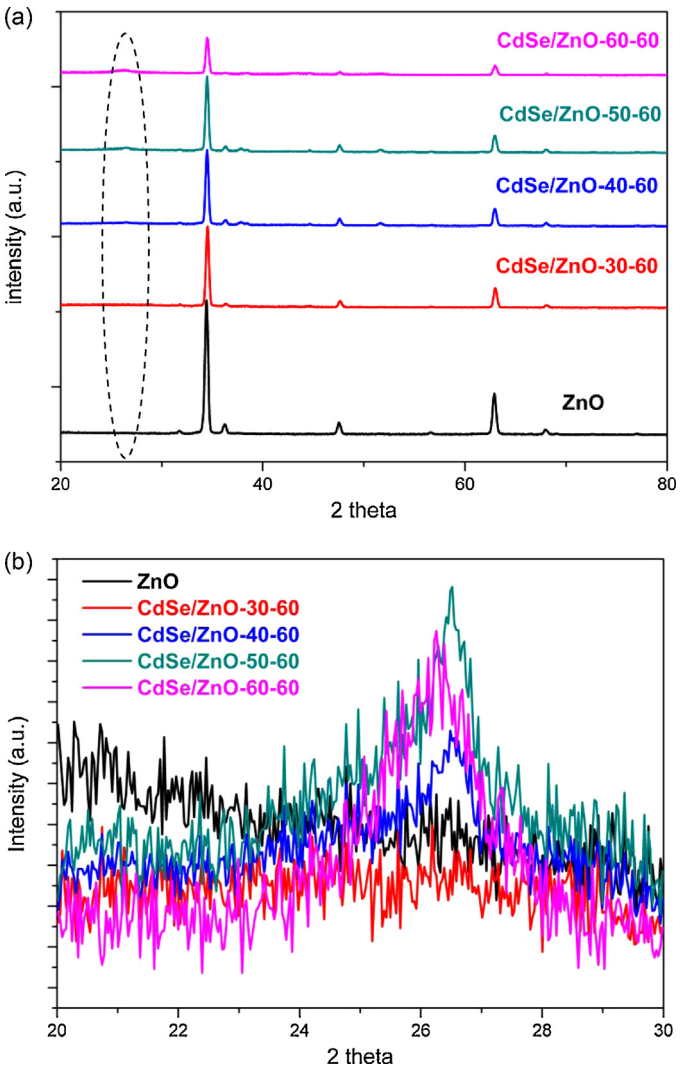

Fig. 3. (a) XRD patterns of CdSe/ZnO nanostructure arrays prepared at different temperatures with the data of ZnO as a reference and (b) XRD patterns of the samples as the diffraction angle changed from 20° to 30°.

energy. Meanwhile, the {1 0 1 0} planes are composed of equivalent O^{2-} and Zn^{2+} ions at the same planes, thus the {1 0 1 0} planes have the lowest surface energy. The different electronic structures of these surfaces result in a distinguishing chemical stability. It has been proved that the stability of ZnO planes can be described as (1 0 1 0) > (0 0 0 1)-Zn > (0 0 0 1)-O. Accordingly the difference of

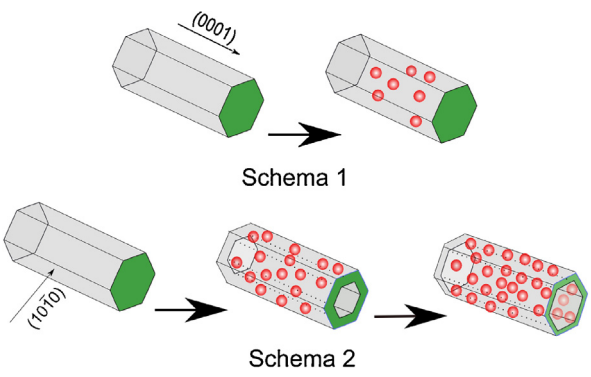

Fig. 4. Schematic of the growth mechanism of double layer nanostructure arrays synthesized by the chemical bath method.

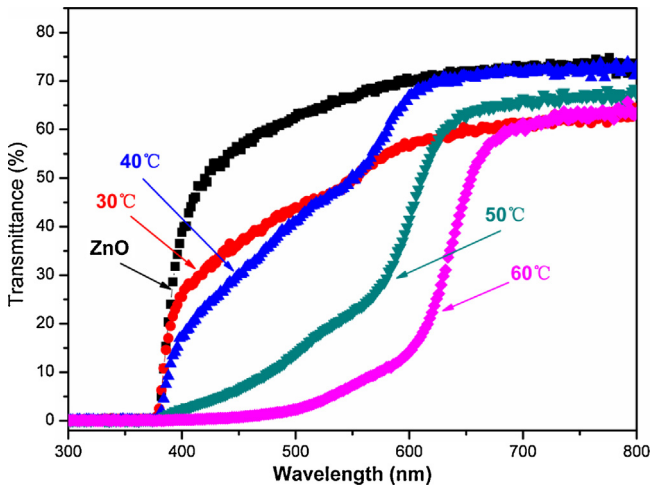

Fig. 5. Transmission spectra of ZnO and CdSe/ZnO nanostructure arrays grew at different temperatures (30 °C, 40 °C, 50 °C, 60 °C) and same time (60 min).

selective dissolution speed between series ZnO planes result in the formation of the tubular ZnO nanostructure [34]. Finally, double layered tubular nanostructure was formed by the stacking of CdSe quantum dots around the ZnO rods and the etching of central part of hexagonal ZnO.

3.3. Optical characteristics

The transmission spectra are given in Fig. 5. The absorption onset for ZnO was around 370 nm corresponding to a band gap of 3.37 eV, indicating that only ultraviolet light could be absorbed by ZnO nanorods. Fig. S4 shows the absorption spectrum of CdSe powder collected from the reaction solution after the deposition process at 60 °C for 60 min. The absorption edge was around 675 nm. And the band gap of CdSe collected after CdSe depositing at 60 °C for 60 min was calculated to be about 2.04 eV by K–M method [35]. The absorption edge shifted significantly to the visible region, after the depositing of CdSe on ZnO surface and etching of the ZnO central part. By increasing the reaction temperature, more CdSe could be deposited on the ZnO surface, which caused more marked red shift of absorption edges of CdSe/ZnO. By depositing pre-synthesized CdSe quantum dots on TiO_2 films, a similar improvement of the absorption capability which is assigned to CdSe quantum dot was also observed by Robel et al. [36]. All these results showed that CdSe/ZnO nanostructure arrays thus-prepared (by combing the absorption ability of ZnO in UV region and absorption ability of CdSe in visible region) could utilize both UV and visible light of the solar spectrum.

3.4. Element analysis

Element analysis of the as-prepared films was performed by the energy-dispersive X-ray (EDX) spectrum, and the data of CdSe/ZnO-60-60 (inset, Fig. S2) is presented as an example. The spectrum showed the signals of O, Zn, Se and Cd. What is more the atom ratios of Zn to Cd of CdSe/ZnO prepared with different reaction conditions were shown in Table 1. The ratio of Zn to Cd was 89.09 for the sample prepared at 30 °C for 60 min indicating that very little CdSe deposited on the ZnO nanorods (Fig. 1a). However, the ratio decreased significantly as reaction temperature raised. When the reaction temperature was increased to 60 °C, the Zn to Cd ratio decreased to 1.88 because the central part of ZnO nanorods etched easily and more CdSe quantum dots were deposited on the ZnO nanorods at present reaction condition, which could be confirmed by the SEM image and TEM image. The atom ratio of Zn to Cd

Table 1
The atom ratio of Zn to Cd, photocurrent performance and photoconversion efficiency of as-prepared CdSe sensitized ZnO nanostructure arrays.

Samples	Photocurrent (mA/cm^2)[a]	Photoconversion efficiency[a]	Atom ratios of Zn to Cd of the samples
CdSe/ZnO-30-60	0.56	0.3%	89.09
CdSe/ZnO-40-60	0.7	0.46%	19.33
CdSe/ZnO-50-60	1.1	0.9%	13.67
CdSe/ZnO-60-60	2.55	1.78%	1.88
CdSe/ZnO-60-100	0.61	0.6%	1.50

[a] The photoelectrochemical measurement was carried out in a convenient three electrodes cell with 0.1 M Na_2S aqueous solution as the electrolyte. The surface areas exposed to electrolyte were fixed at 0.785 cm^2. A silver chloride electrode was used as a reference electrode and a large area platinum plate was used as a counter electrode. What is more a chopped light illumination of 100 mW/cm^2 was used as the light source.

decreased too as reaction time extended. Consequently the tubular morphology of CdSe/ZnO-60-100 (Zn to Cd ratio is 1.5) was more distinct than that of CdSe/ZnO-60-60 (Zn to Cd ratio is 1.88) (Fig. 1c and d).

3.5. Photoelectrochemical properties

Fig. 6 shows the chopped photocurrent–potential curves of the as-prepared CdSe/ZnO nanostructure arrays, and the curve of ZnO is also shown as a reference. Dark current density for all samples can be neglected. While upon irradiation, the photocurrent increased significantly. Photocurrent onset of ZnO nanorods was at about −0.52 V. However, for CdSe/ZnO nanostructure arrays photocurrent onset was at about −1.1 V. And it is well known that conduction band of most n-type semiconductors is about 0.1–0.3 V more negative than flat band [37,38]. Thus the edge of conduction band (ECB) of CdSe is more negative than that of ZnO. Photoelectrons in CdSe caused by irradiation of visible light could inject to the conduction band of ZnO immediately, which result in higher separation efficiency and longer life time for photo-generated charges. It can be seen from Fig. 6a and b that ZnO showed a photocurrent value of 210 μA/cm^2 with applied potential of 0 V vs Ag/AgCl. With the increase of reaction temperature and time, the photocurrent increased gradually. Photocurrent of CdSe/ZnO-60-60 is about 2.55 mA/cm^2 over 12 times than that of ZnO. However CdSe/ZnO-70-60 and CdSe/ZnO-60-80 gave lower photocurrent than CdSe/ZnO-60-60. This may be due to more ZnO nanorods dissolved in experimental solution at such reaction condition, so the photoelectrons generated from CdSe were not able to inject to ZnO opportunely. As a result a lot of electrons and holes recombined on CdSe particles.

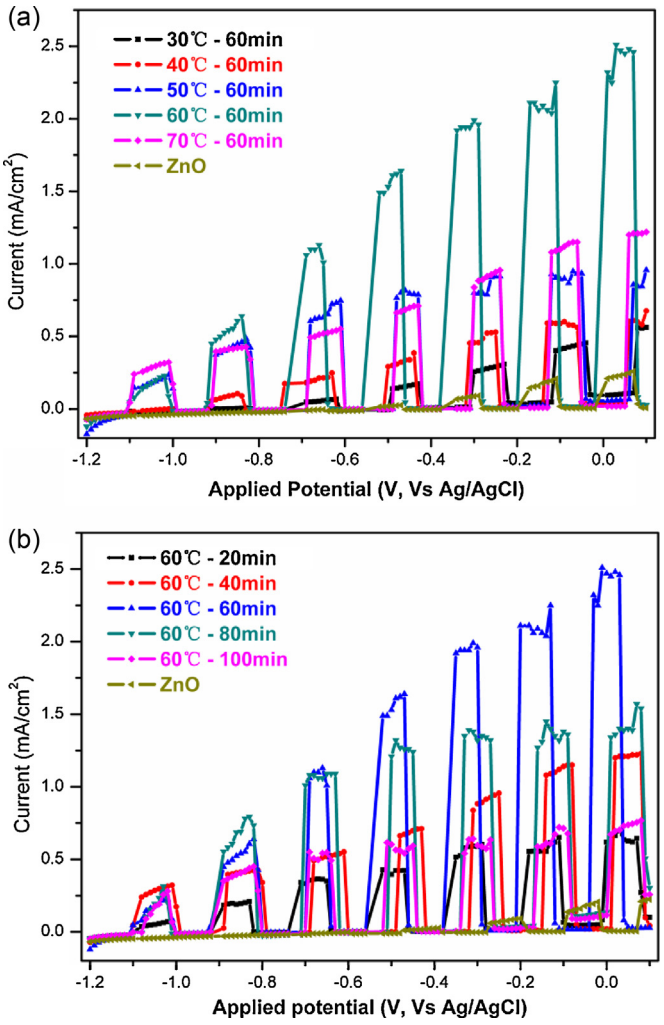

Fig. 6. Current–potential plots of as-prepared CdSe/ZnO films (a) synthesized at same time and different temperatures and (b) synthesized at same temperature and different time. Current–potential plot of ZnO is also shown as a reference.

To study the photoeletrochemical performance at different wavelengths of various photoelectrodes, IPCE measurement was performed in 0.1 M of Na_2S aqueous solution at an applied potential of 0 V vs Ag/AgCl, which is shown in Fig. S6. As compared to bare ZnO, the onsets of the spectra for CdSe sensitized ZnO give significantly red shift. ZnO electrode responded to the incident light with wavelength smaller than 370 nm, while for CdSe modified electrodes the photoactive region expanded to the wavelength of 700 nm. These results matched well with the transmission spectra as shown in Fig. 5. As the increase of chemical bath deposition temperature, the best IPCE was achieved at about 15% for CdSe/ZnO-60-60. The high IPCE performance was perhaps due to the combined effects of light harvesting of CdSe and superior charges separation efficiency between ZnO and CdSe.

The solar energy to chemical energy conversion efficiency, named as photoconversion efficiency (η) is also shown in this paper and calculated as below [39]

$$\eta\ (\%) = \frac{\text{total power output-electrical input}}{\text{light power input}} \times 100$$

$$= \frac{j_p[E^0_{rev} - |E_{app}|]}{I_0} \times 100 \quad (2)$$

j_p is the photocurrent density (mA/cm^2), $j_pE^0_{rev}$ is total energy output, j_pE_{pp} is the total electrical energy input, and I_0 is the power density of incident light ($mW\,cm^{-2}$). E^0_{rev} refers to the standard reversible potential of 1.23 V [vs the normal hydrogen electrode (NHE)]. The applied potential is $E_{app} = E_{means} - E_{aoc}$, where E_{means} stands for the electrode potential (vs Ag/AgCl) of work electrode at which the photocurrent is measured under irradiation and E_{aoc} is the electrode potential (vs Ag/AgCl) of the same work electrode under open-circuit conditions under the same irradiation and in the same electrolyte (0.1 M of Na_2S solution) [39].

Fig. 7a and b shows the photoconversion efficiency of serial CdSe/ZnO nanostructure arrays synthesized at different reaction conditions, and the curve of ZnO is also shown for reference. Significant increase was observed after depositing CdSe quantum dots onto the ZnO nanorods. As the depositing temperature increased and reaction time extended, photoconversion efficiency of CdSe/ZnO nanostructure arrays increased markedly. When reaction temperature and time increased to 60 °C and 60 min respectively, photoconversion efficiency of CdSe/ZnO reached the maximum of 1.78% which was about 13 times as much as that of ZnO electrode (0.14%). But if the reaction temperature and time

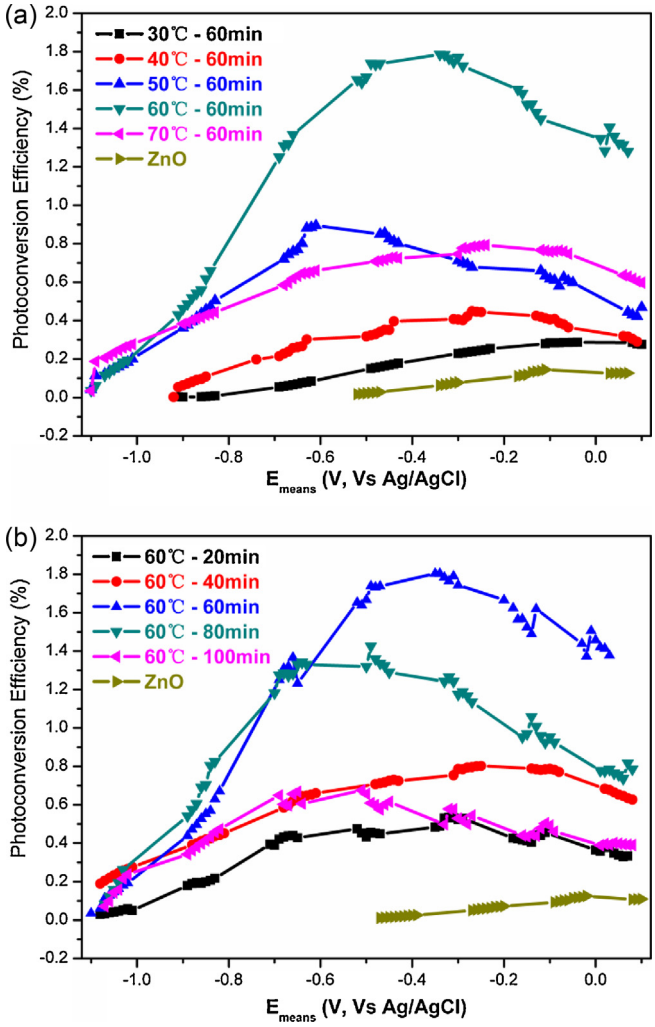

Fig. 7. Photoconversion efficiency for as-prepared CdSe/ZnO nanostructure films (a) synthesized at different temperatures and (b) synthesized at different time as a function of applied potential (vs Ag/AgCl). The curve of ZnO is also shown for reference.

increased furthermore, photoconversion efficiency of CdSe/ZnO films decreased. Photoconversion efficiency of CdSe/ZnO-70-60 and CdSe/ZnO-60-100 were 0.79% and 0.61% respectively.

Fig. 8 displays schematic operation of photocatalytic process of CdSe/ZnO arrays. Both valance band maximum (VBM) and conduction band minimum (CBM) of CdSe lie above that of ZnO. Because of the heterojunction between ZnO and CdSe, photo-generated electrons from CdSe can be injected to the conduction band of ZnO quickly, and then transform to the FTO substrate along the single crystal ZnO nanotube. For this reason, the separation efficiency and life time of photo-generated charges were both improved.

It has been proved by Kislov et al. different crystal planes of ZnO show different photocatalytic activities and stabilities [40]. The results showed that, the photocatalytic activity of ZnO strongly dependent on the crystallographic orientation. The {0 0 0 1} planes exhibit lower photolysis stability and photocatalytic activity than that of {1 0 1 0} planes. CdSe sensitized tubular structure ZnO arrays obtained by our group were mainly composed of stable {1 0 1 0} surface instead of {0 0 0 1} surface. Moreover the tubular structure has a larger specific surface area than rods. According to the analysis provided above, it can be concluded that double layered tubular structure arrays of CdSe sensitized ZnO can achieve better photocatalytic performance, which agrees well with our experimental results.

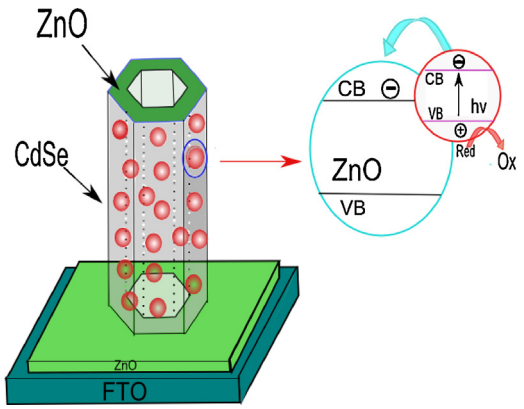

Fig. 8. Schematic operation of photocatalytic process of CdSe/ZnO double layer tubular structure arrays: electrons are injected from excited CdSe quantum dots to ZnO nanotubes, and the tubular shape provide a direct pathway for electrons transform from ZnO to FTO substrate.

4. Conclusions

A series of CdSe/ZnO nanostructure arrays grew on the FTO substrate were synthesized by the chemical bath deposition method using as-prepared ZnO nanorods as the template. The micro-nanostructures can be controlled by changing the experimental conditions. As the reaction temperature and reaction time increased, the morphology changed from nanocable to double layered nanotube, and CdSe/ZnO of this nanostructure was synthesized by the present method for the first time. Structural and electrical properties of this material were investigated to describe their effects for PEC performance. CdSe/ZnO film with this double layered tubular structure gives the highest photocurrent of 2.55 mA/cm^2 and highest photoconversion efficiency of 1.78% under the illumination of 100 mW/cm^2. This approach to design novel 1D nanostructure films will give a new direction in various fields including catalysis, gas detection, electrochemistry, purification and so on.

Acknowledgements

This work was supported by the Natural Science Foundation of China (No. 51121092 and No. 91010012), the National Basic Research Program of China (No. 2009CB220000).

Appendix A. Supplementary data

Supplementary data associated with this article can be found, in the online version, at http://dx.doi.org/10.1016/j.apcatb.2013.02.027.

References

[1] A. Fujishima, K. Honda, Nature 238 (1972) 37–38.
[2] J. Su, L. Guo, S. Yoriya, C.A. Grimes, Crystal Growth & Design 10 (2010) 856–861.
[3] J. Su, X. Feng, J.D. Sloppy, L. Guo, C.A. Grimes, Nano Letters 11 (2011) 203–208.
[4] M. Koinuma, H. Seki, Y. Matsumoto, Journal of Electroanalytical Chemistry 531 (2002) 81–85.
[5] E. Evgenidou, K. Fytianos, I. Poulios, Applied Catalysis B: Environmental 59 (2005) 81–89.
[6] J. Shi, J. Ye, Q. Li, Z. Zhou, H. Tong, G. Xi, L. Guo, Chemistry: A European Journal 18 (2012) 3157–3162.
[7] D. Jing, L. Guo, L. Zhao, X. Zhang, H. Liu, M. Li, S. Shen, G. Liu, X. Hu, X. Zhang, International Journal of Hydrogen Energy 35 (2010) 7087–7097.
[8] Q. Li, Y.W. Li, P. Wu, R. Xie, J.K. Shang, Advanced Materials 20 (2008) 3717–3723.

[9] K. Zhang, D.W. Jing, C.J. Xing, L.J. Guo, International Journal of Hydrogen Energy 32 (2007) 4685–4691.
[10] J.S. Jang, D.J. Ham, N. Lakshminarasimhan, W.Y. Choi, J.S. Lee, Applied Catalysis A: General 346 (2008) 149–154.
[11] A. Kudo, Y. Miseki, Chemical Society Reviews 38 (2009) 253–278.
[12] R. Huirache-Acuna, F. Paraguay-Delgado, M.A. Albiter, L. Alvarez-Contreras, E.M. Rivera-Munoz, G. Alonso-Nunez, Journal of Materials Science 44 (2009) 4360–4369.
[13] M. Liu, L. Wang, G. Lu, X. Yao, L. Guo, Energy & Environmental Science 4 (2011) 1372.
[14] M. Yashima, K. Maeda, K. Teramura, T. Takata, K. Domen, Chemical Physics Letters 416 (2005) 225–228.
[15] K. Kamata, K. Maeda, D. Lu, Y. Kako, K. Domen, Chemical Physics Letters 470 (2009) 90–94.
[16] K. Domen, Solar Hydrogen and Nanotechnology III 7044 (2008) J440.
[17] U.G. Akpan, B.H. Hameed, Applied Catalysis A: General 375 (2010) 1–11.
[18] E. Borgarello, J. Kiwi, M. Grätzel, E. Pelizzetti, M. Visca, Journal of the American Chemical Society 104 (1982) 2996–3002.
[19] M. Li, J. Su, L. Guo, International Journal of Hydrogen Energy 33 (2008) 2891–2896.
[20] K. Sunahara, A. Furube, R. Katoh, S. Mori, M.J. Griffith, G.G. Wallace, P. Wagner, D.L. Officer, A.J. Mozer, The Journal of Physical Chemistry C 115 (2011) 22084–22088.
[21] M. Ziółek, C. Martín, B. Cohen, H. Garcia, A. Douhal, The Journal of Physical Chemistry C 115 (2011) 23642–23650.
[22] M.K.I. Senevirathna, P. Pitigala, K. Tennakone, Journal of Photochemistry and Photobiology A: Chemistry 171 (2005) 257–259.
[23] S. Banerjee, S.K. Mohapatra, P.P. Das, M. Misra, Chemistry of Materials 20 (2008) 6784–6791.
[24] Y.-L. Lee, C.-F. Chi, S.-Y. Liau, Chemistry of Materials 22 (2010) 922–927.
[25] T.K. Sung, J.H. Kang, D.M. Jang, Y. Myung, G.B. Jung, H.S. Kim, C.S. Jung, Y.J. Cho, J. Park, C.-L. Lee, Journal of Materials Chemistry 21 (2011) 4553.
[26] O. Niitsoo, S.K. Sarkar, C. Pejoux, S. Rühle, D. Cahen, G. Hodes, Journal of Photochemistry and Photobiology A: Chemistry 181 (2006) 306–313.
[27] C. Borchers, S. Müller, D. Stichtenoth, D. Schwen, C. Ronning, The Journal of Physical Chemistry B 110 (2006) 1656–1660.
[28] J.Y. Li, H. Li, Nanoscale Research Letters 4 (2008) 165–168.
[29] X. Wang, H. Zhu, Y. Xu, H. Wang, Y. Tao, S. Hark, X. Xiao, Q. Li, ACS Nano 4 (2010) 3302–3308.
[30] Y. Sun, G.M. Fuge, N.A. Fox, D.J. Riley, M.N.R. Ashfold, Advanced Materials 17 (2005) 2477–2481.
[31] L.E. Greene, M. Law, J. Goldberger, F. Kim, J.C. Johnson, Y. Zhang, R.J. Saykally, P. Yang, Angewandte Chemie International Edition 42 (2003) 3031–3034.
[32] M. Zhou, H. Zhu, X. Wang, Y. Xu, Y. Tao, S. Hark, X. Xiao, Q. Li, Chemistry of Materials 22 (2010) 64–69.
[33] D. Chu, Y. Masuda, T. Ohji, K. Kato, Langmuir 26 (2010) 2811–2815.
[34] J. Han, F. Fan, C. Xu, S. Lin, M. Wei, X. Duan, Z.L. Wang, Nanotechnology 21 (2010) 405203.
[35] F. Gao, X.Y. Chen, K.B. Yin, S. Dong, Z.F. Ren, F. Yuan, T. Yu, Z.G. Zou, J.M. Liu, Advanced Materials 19 (2007) 2889–2892.
[36] I. Robel, V. Subramanian, M. Kuno, P.V. Kamat, Journal of the American Chemical Society 128 (2006) 2385–2393.
[37] W.J. Chun, A. Ishikawa, H. Fujisawa, T. Takata, J.N. Kondo, M. Hara, M. Kawai, Y. Matsumoto, K. Domen, Journal of Physical Chemistry B 107 (2003) 1798–1803.
[38] Y. Matsumoto, Journal of Solid State Chemistry 126 (1996) 227–234.
[39] X. Li, Y. Hou, Q. Zhao, G. Chen, Langmuir 27 (2011) 3113–3120.
[40] N. Kislov, J. Lahiri, H. Verma, D.Y. Goswami, E. Stefanakos, M. Batzill, Langmuir 25 (2009) 3310–3315.
[41] W. Zhao, W. Ma, C. Chen, J. Zhao, Z. Shuai, Journal of the American Chemical Society 126 (2004) 4782–4783.
[42] J. Shi, L. Guo, Progress in Natural Science: Materials International 22 (2012) 592–615.